J Mater Sci (2010) 45:4480–4489
DOI 10.1007/s10853-010-4532-2

Effect of process conditions on phase mixtures of sol–gel-synthesized nanoscale orthorhombic, tetragonal, and monoclinic zirconia

Miriam P. Trubelja · Donald Potter · Joseph J. Helble

Received: 22 December 2009 / Accepted: 15 April 2010 / Published online: 1 May 2010

Abstract Zirconia particles synthesized under ambient conditions are frequently amorphous, requiring heat to produce a crystalline phase. Synthesized nanoparticles are generally found in the tetragonal phase. In this article, a room temperature sol–gel synthesis of crystalline sub-10-nm zirconia particles is described. By adjusting the acid concentration of the reaction, it is found that the particles' crystalline phase can be modified. Under acidic conditions with moisture present, the tetragonal phase is produced, whereas under acidic conditions with low water content, 2–5-nm particles suggestive of the metastable orthorhombic phase are produced. Subsequent heat treatment of all powders produced with this technique resulted in their transformation first to the tetragonal phase, and ultimately to the monoclinic phase. The extent of the transformation to the monoclinic phase depends upon the atmosphere, however, suggesting that oxygen vacancies play a significant role in the stabilization and determination of the resulting phase.

M. P. Trubelja · J. J. Helble
Department of Chemical Engineering, University of Connecticut, Storrs, CT 06269-3136, USA
e-mail: Trubela@att.net; Trubelja@att.net

D. Potter
Department of Materials Science and Engineering, University of Connecticut, Storrs, CT 06269-3136, USA
e-mail: DONALD.POTTER@uconn.edu

J. J. Helble (✉)
Thayer School of Engineering at Dartmouth, 8000 Cummings Hall, Hanover, NH 03755-8000, USA
e-mail: Joseph.Helble@Dartmouth.edu

Introduction

Unstabilized ZrO_{2-x}, where $0 < x < 0.44$, is known to exist in three different structures at ambient pressure. At low temperatures (<1500 K), the monoclinic baddeleyite structure (P21/c) is thermodynamically favored. At intermediate temperatures, the tetragonal phase (P42/nmc) is favored, and at temperatures of 2650 K up to the melting point, the cubic fluorite structure (Fm3m) is dominant [1].

At ambient temperatures and elevated pressures above 3.5 GPa, unstabilized zirconia can also exist as an orthorhombic structure [2, 3]. As temperature increases, there is a decrease in the pressure required for the appearance of the orthorhombic phase [4]. The first two orthorhombic structures above ambient pressure [5–7] are Ortho I and Ortho II. The first, Ortho I, which was found to be stable at ambient temperature and pressures ranging from approximately 3.5 to 16.6 GPa, is a brookite (Pbca) structure [8, 9]. This particular phase has been shown to be similar to the tetragonal phase, both slight variants of the cubic fluorite structure [5, 10, 11]. A second orthorhombic phase, Ortho II, stable at pressures above 19.0 GPa, possesses a cotunnite (Pnma) [12] structure. The only cotunnite structure produced at room temperature [12] was found to start transforming from the brookite structure at 16.6 GPa and had completed its transformation at a pressure of 22.0 GPa. Three other forms of orthorhombic zirconia have also been synthesized: Ortho III ($Pbc2_1$: $T = 30$–573 K, $P = 42$ Gpa [9]) Ortho IV ($P2_12_12_1$: $T = 293$, $P = 37.5$–42.5 GPa) [12], and Ortho V (Pmnb: Quenched from $T = 1298$ K, $P = 20$ GPa) [13] and (P42/nmcz: $T =$ N/A, $P = 214$ GPa) [14].

While zirconia exists as the stable monoclinic phase at ambient pressure and temperature, metastable forms of the material also exist under these conditions when the crystallites are in the nanoscale range. These metastable

particles are generally tetragonal or cubic phases [15–21]. Although the literature clearly demonstrates the feasibility of producing metastable phases under a broad range of conditions, reports of the synthesis of other metastable phases of nanoscale zirconia at ambient conditions are limited. Most reports citing the preparation of orthorhombic zirconia make use of stabilizing agents [8–11, 22–24].

Rossignol et al. [25] have suggested that unstabilized orthorhombic zirconia could be produced by the 873 K heat treatment of amorphous powders produced from sol–gel synthesis using zirconium propoxide. Troilliard et al. have succeeded in synthesizing small islands ($d > 100$ nm) of unstabilized orthorhombic zirconia on sapphire thin film substrates at high temperature (1773–1973 K) [26]. While this offers intriguing possibilities, synthesis at elevated temperature and pressure was not the focus of this investigation and thus was not explored in these studies.

The objective of this study is to explore the feasibility of synthesizing unstabilized orthorhombic zirconium oxide powder at ambient temperature and pressure. Orthorhombic zirconium oxide has a high-pressure room temperature phase that is more stable to thermal cycling than the ambient monoclinic phase. This material also yields a much smaller volume change upon thermal transformation to the tetragonal structure as compared to the monoclinic phase. Calculations using the Young–Laplace Equation suggested that the internal pressure of a particle, where the room temperature orthorhombic phase [2, 3] might be stable, would be only in the nanoscale form. For these reasons, it was hypothesized that orthorhombic zirconia might be a suitable thermal barrier coating material if (a) it could be synthesized in powder form, and (b) it possessed suitable thermal and mechanical stability. Therefore, the major effort in this study focused on synthesizing and characterizing the structure of the nanometer orthorhombic zirconia powder.

The sol–gel synthesis of metastable nanoscale zirconia used to achieve this goal is described in this article. Synthesis experiments were conducted using initially anhydrous solvent at a range of acid concentrations to control crystal and particle (agglomerate) size and crystal phase. Exploration of a broad range of conditions permitted synthesis of particles in the tetragonal phase, and provided evidence supportive of the orthorhombic phase in some samples.

Experimental

Synthesis

Literature reports on the synthesis of nanoscale ZrO_2 suggested that the smallest particles would be produced by a method generally referred to as a sol–gel process [20, 21]. In this study, syntheses were conducted using an organometallic zirconium precursor, zirconium(IV) *n*-butoxide ($Zr(OC_4H_9)_4$), with the homologous alcohol, anhydrous 1-butanol (Fisher Scientific, Pittsburgh), as the system solvent and 0.94-M nitric acid (Fisher Scientific, Pittsburgh) solution as the initiator.

To synthesize the particles, 100 mL of anhydrous 1-butanol were added to a clean polypentene beaker. As the solution was stirred, from 400 to 2000 μL of 0.94-M HNO_3 were added. Immediately after addition of the 0.94-M HNO_3, wax film was used to seal the beaker to prevent further exposure to atmospheric moisture and the solution was then transferred to a nitrogen glove box. After 20 min, the wax film was removed from the beaker and 410 μL of zirconium-*n*-butoxide were added by pipette to the stirred 1-butanol solution. A small amount (7 mL) of solution was removed and stored in a chemical refrigerator (278 K) for subsequent characterization. Wax film was placed over the beaker, and the nitrogen flow to the glove box was then discontinued.

To produce a dry powder sample, the remainder of the sol–gel solution was evaporated on a hot plate in a hood at a moderate temperature ($\sim$343–353 K) while being stirred at approximately 300–350 rpm. Evaporation to dryness required approximately 24 h. Approximately 70 mg of a semi-translucent yellow-orange powder were deposited on the bottom of the beaker after drying. All the powder samples synthesized for analysis were dried in this manner. In experiments in which the particle size distribution of the powders was measured in solution by dynamic light scattering, a portion of the sample was removed prior to the evaporation step.

Synthesis experiments were carried out with varying amounts of 0.94-M HNO_3 to determine the effect of acid and water content on particle formation. A single synthesis was also conducted using 15.8-M HNO_3 to determine the effect of the increased acid concentration. Table 1 contains detailed information of concentrations for water and HNO_3 in each synthesis experiment.

Table 1 Concentration values for water and initiator used in each synthesis solution

Initiator concentration (M)	Volume initiator used (μL)	Volume HNO_3 (μL)	Water (mol)
0.94	400	15.76	0.0213
0.94	800	31.52	0.0426
0.94	1200	47.28	0.0639
0.94	1600	63.04	0.0852
0.94	2000	78.80	0.1066
15.8	2000	1324	0.0375

Analytical

Particle sizes were measured by dynamic light scattering (DLS) using a Brookhaven Instruments BI9000-AT autocorrelator (BIC, Holtsville, NY). The light source was a Coherent Innova 70-3 Ar+ laser (Coherent Inc., Santa Clara, CA) operating at 514.5 nm. Measurements were made at an angular range of 20°–150° provided by a Brookhaven BI200SM goniometer under computer control. DLS was used to determine the average size of a suspended population of particles or clustered particles in the dilute sol–gel solution. Each DLS measurement was made 1 h after particle synthesis, and thus provided a snap-shot of the average particle size at a given time. Samples were typically analyzed by DLS for a period of 1.5 h.

High-resolution TEM was also conducted on selected samples at the High Temperature Materials Lab (HTML) at Oak Ridge National Laboratory (ORNL). A Hitachi HF-2000 High-Resolution Transmission Electron Microscope (HRTEM; HHTA, San Jose CA) was used to image the particles. Samples for HRTEM measurements were deposited on holey carbon TEM grids. The samples were prepared by drying several drops of the sol–gel solution on a glass slide set on a hot plate for 20 min. The resulting dried powders were scraped off the glass slide into a vial of isopropanol and allowed to soak overnight, since initial attempts to image the crystallites were hampered by excessive amounts of gel surrounding the crystallites. A drop of the isopropanol solution was then placed onto the holey carbon TEM grid and allowed to air dry for 3–4 min prior to analysis.

Samples for HRTEM analysis were synthesized in the presence of 2000, 1600, 1200, 800, and 400 μL 0.94-M HNO_3 acid concentrations. Digital micrographs were taken at varying magnifications to examine both the size and the morphology of the synthesized material. Diffractograms were then made from the digitized TEM images. Distance between the center of the diffractogram to a diffraction spot was then digitally measured. Equation 1 was then used to calculate interplanar spacing.

$$d\ (\mathrm{nm}) = \frac{25.4 * 10^3}{K_{\mathrm{mag}} * F * N * D} \quad (1)$$

where N is the Fast Fourier Transform (FFT) size factor, d is the d-space of the crystal structure in nanometers, D is the distance from a diffraction spot to the center in diffractogram (in pixel value), F is the image size factor between film plate and CCD camera, and K_{mag} is the magnification shown on TEM (in ×1000).

Particle size and morphology were also examined by transmission electron microscopy (TEM). TEM samples were prepared by thermophoretic deposition on thin films of carbon-coated copper TEM grids, accomplished by dipping the grids in liquid nitrogen for approximately 2 s and then rapidly immersing them in the sol–gel solution. Grids were held in the sol–gel solution for 3–4 s before removal. TEM (Philips Model 420, The Netherlands) was used to image the ZrO_2 particles and perform selected area electron diffraction. Electron diffraction patterns calculated for different reference structures were then compared with the electron diffraction patterns obtained from the synthesized material. Norelco/Philips and Bruker diffractometers were used to determine the structure of the synthesized ZrO_2 by X-ray diffraction.

To determine the effect of varying atmospheres and temperature regimes on the as-synthesized zirconia powders, a series of XRD runs were carried out at HTML, using a Scintag PADX vertical Θ/2Θ goniometer equipped with a modified Buehler HDK-2 diffraction furnace, using Cu Kα radiation (45 kV and 40 mA) and an Si(Li) Peltier cooled solid state detector. Powder samples were dispersed on a Pt/Rh heater strip with the control thermocouple spot welded to the bottom of the heater strip. Thermal gradients were expected through the thickness, as well as the length of the sample, making the actual temperature less than that of the control thermocouple. The sample temperature was checked using an optical pyrometer. Data were collected as step scans, with a step-size of 0.02° 2Θ, at a scan rate of 1°/min, between 25° and 60° 2Θ. Samples were run under (1) bottled air, (2) ungettered argon (30 ppm O_2), (3) titanium gettered argon, and (4) vacuum. XRD data were taken from 298 to 1373 K, with increasing temperature increments of 50 K. The heating rate used was 25 K/min, with a 60-s hold time to stabilize the temperature. The scan time required for each XRD pattern was 35 min. At the completion of each scan the temperature was again immediately increased.

The International Center for Diffraction Data (ICDD) patterns for Powder Diffraction Files (PDF) was used to identify the crystal phase(s) present. The X-ray powder diffraction patterns showed peak broadening, due to small crystallite size (<1-μm diameter). An amorphous pattern was identified for the 2000 μL, 15.8-M samples by the complete lack of any peak regions. A peak-fitting program provided with the Bruker Analytical X-Ray System was used to determine the average crystallite size of zirconia powders, where clearly defined, individual 2Θ peaks could be identified. Profile fitting used the Pseudo-Voigt function to model the XRD pattern and determine the average crystallite size using the Scherrer formula [27, 28].

Surface areas measured by BET techniques were also obtained for selected samples as a secondary means of particle size characterization. The powders characterized using this method included the as synthesized and dried at around 343–353 K on a hot plate, and heat treated at 473, 673, 873, 1073, and 1273 K in a furnace open to the

Table 2 BET nitrogen adsorption for specific surface areas for heat treated samples

Heat treatment temperature (K)	Outgassing temperature (K)	Outgassing time (h)	Specific surface area (m^2/g)	Average crystallite diameter (nm)
1200 μL, as synthesized	393	1.0	187	–
473	393	0.5	426	2.68
673	393	1.0	556	2.05
873	393	0.75	268	4.26
1073	393	0.75	154	7.41
1273	393	1.0	156	7.31

atmosphere for a period of 1 h. Measurements were made using five-point nitrogen adsorption on a Quanta chrome NOVA 1000 instrument (Quanta chrome Instruments, Boynton Beach, FL). Table 2 provides the experimental conditions under which each sample was measured.

The available system for determining surface area possessed the capacity to neither determine the porosity of the material nor record the adsorption isotherms of the run. Sample weights were measured prior to each run using a Mettler scale and then placed in the equipment, degassed and surface area measured. The value for each powders surface area was manually recorded from the digital readout on the equipment and specific surface area calculated (Table 2). Future study is planned to fully characterize pore size distribution and provide adsorption isotherms.

Phase transitions within the as synthesized, low temperature dried samples were identified through a combination of differential thermal analysis (DTA), differential scanning calorimetry (DSC), and thermogravimetric analysis (TGA). A Simultaneous Thermal Analyzer 409 Netzsch DTA and TGA (Netzsch Instruments Inc., Burlington, MA) was used to perform tests over a temperature range of 298–1773 K. Tests were conducted under an argon atmosphere in a sealed chamber, with a contained atmosphere (no gas exchange), at a heating rate of 10 K/min. A second DTA analysis was also conducted on selected samples at a commercial laboratory (M&P Laboratories, Schenectady). These latter measurements were conducted both under flowing argon (50 mL/min) and under flowing air at a heating rate of 10 K/min.

Results and discussion

Particle size and crystallinity

From DLS measurements, it was found that particles of 2–5 nm had been synthesized using 2000 μL of 0.94-M nitric acid. The effect of decreasing the amount of 0.94-M nitric acid was to increase the size of the particles. Results indicated that the average particle sizes for 2000, 1600, 1200, and 800 μL of 0.94-M nitric acid were 3.5, 12.5, 15.0, and 84 nm, respectively. For the synthesis performed using 15.8-M nitric acid, dynamic light scattering determined the average diameter of the particles to be slightly less than 2.0 nm.

As-prepared samples synthesized at concentrations of 2000, 1600, 1200, 800, and 400 μL of 0.94-M nitric acid were examined by HRTEM. It was found that even with a change in the amount of 0.94-M HNO_3 used; primary particle diameters remained within a narrow size range of approximately 2–5 nm as shown in the micrograph in Fig. 1. Aggregate sizes were, however, found to increase with a decrease in the amount of 0.94-M HNO_3 used, in agreement of the overall trends determined by DLS.

In addition, the HRTEM micrographs also established the fact that all the particles synthesized at concentrations of 2000, 1600, 1200, 800, and 400 μL of 0.94-M nitric acid were fully crystalline. This is evident from the cross hatch pattern within the particles, indicative of the presence of a crystal lattice, and clearly visible in Fig. 1. Surrounding the crystallites is the holey carbon film on which the particles were supported.

XRD analysis of these samples indicated that for the material synthesized using 2000, 1600, and 1200 μL amounts of 0.94-M nitric acid, the as-synthesized powders did not produce a distinct diffraction pattern. Rather, two distinct broad peaks were observed. As these peaks were broad, the patterns were suggestive of a crystalline material and were consistent with particles small enough to cause sufficient broadening such that peaks close to one another

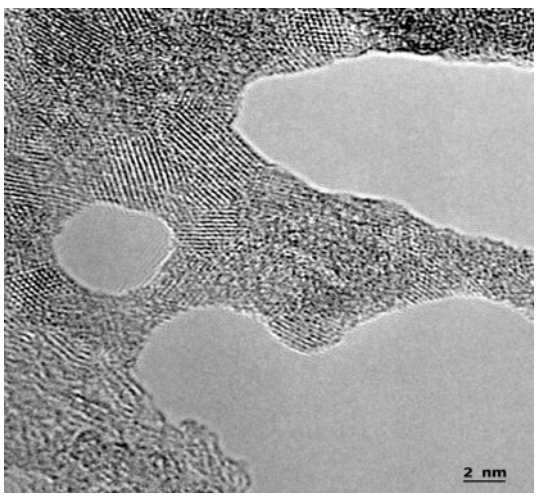

Fig. 1 HRTEM images of as-synthesized zirconia, synthesized with 2000 μL of 0.94-M HNO_3. The *bar* in the figure is 2 nm. The *lined/cross hatched* areas are crystalline

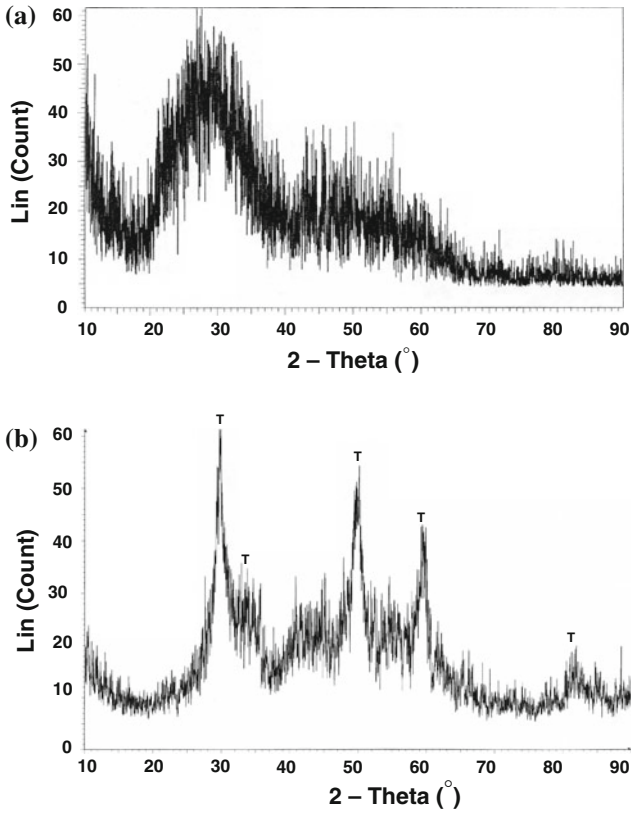

Fig. 2 Raw XRD pattern for as-prepared sample of zirconia synthesized with **a** 2000 μL of 0.94-M HNO_3 and **b** 800 μL of 0.94-M HNO_3. The average particle size was determined to be 3.5 nm using dynamic light scattering. Particle agglomerates of gel and crystallites were found to be 84 nm using dynamic light scattering. The average crystallites were found to be 3.5 nm using peak broadening measurements

would convolve into broad overlapping regions as shown for the sample using 2000 μL of 0.94-M nitric acid in Fig. 2a. This is supported by HRTEM micrograph for a sample synthesized using microliter of 0.94-M nitric acid in Fig. 1, which has established the presence of crystalline particles in the sample. XRD results for the as synthesized 800 μL of 0.94-M nitric acid sample showed a distinct pattern that corresponded to the tetragonal zirconia structure (Fig. 2b).

From PDF cards containing the XRD patterns of all the known structures of zirconium oxide, only two patterns were found which could account for the convolved peaks seen in Fig. 2a. These two possible crystal structures might be either a high-pressure form of orthorhombic zirconia found at high temperature (1300 K) [29] or a tetragonal structure [30]. Comparison of the XRD powder diffraction patterns in Fig. 2a, b against the reference patterns immediately identifies Fig. 2b as the tetragonal structure. The peak fitting program available with the Scintag system determined the average particle size to be 3.5 nm. Also, since the average particle size in Fig. 2a, b were determined to have the same average diameter of 3.5 nm from the HRTEM micrographs, there would have been little variation between the two XRD patterns had they been the same structure. Therefore, the match between Fig. 2b with the tetragonal structure XRD pattern eliminates this phase as the structure for Fig. 2a. This leaves only the high temperature and pressure pattern as the most likely form of the zirconia found in Fig. 2a.

Single particles, imaged with the TEM, were examined using selected area electron diffraction. A pattern from a particle synthesized under conditions of 2000 μL of 0.94-M nitric acid is presented in Fig. 3. Electron diffraction patterns were calculated [31] for the three possible zirconia structures synthesized. Though the three patterns generated appeared to be similar, the ratios of the distance between spots in the horizontal direction to distance between spots in the vertical direction differ significantly. The spacing ratio in the experimentally recorded pattern (A/B = 1.9), matched the generated pattern for the orthorhombic (A/B = 1.9) cotunnite structure. The ratios found for the tetragonal (A/B = 1.53) and monoclinic (A/B = 1.03) structures were significantly different than the experimental pattern. Further, when the selected area diffraction micrograph was laid directly on the generated pattern, each of the diffraction spots fit precisely over the calculated pattern. Thus, the selected area diffraction pattern for these particles matches that of the high pressure and temperature form of zirconia (cotunnite), found just above the room temperature

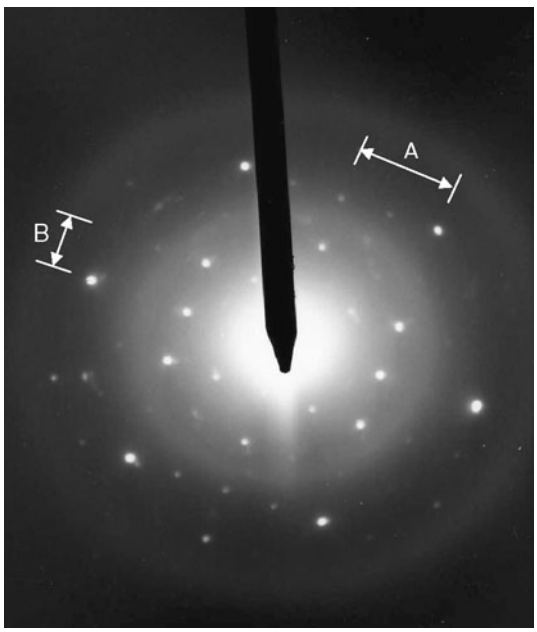

Fig. 3 A single particle selected area electron diffraction pattern for as-synthesized zirconia. The average ratio of the measured distances between each sides primary diffraction spots is $A/B = 1.9$

phase (brookite) and is normally found starting at 16.6 GPa, at temperatures around 1300 K.

It was also noted that the diffraction pattern contains primary reflections weaker than those predicted in the calculated pattern. Secondary reflections can also be observed in the pattern of Fig. 3. The most likely explanation is that these secondary reflections are caused by ordering of oxygen vacancies present within the structure. Selected area diffraction patterns were also examined for as-synthesized particles under conditions of 2000, 1600, and 1200 μL of 0.94-M nitric acid. Selected area electron diffraction patterns similar to Fig. 3 were also found for the majority of these samples. Only a tiny minority of selected area diffraction micrographs displayed a pattern similar to the tetragonal structure.

The above interpretation was further supported by analysis of the resulting interplanar spacing measurements made from HRTEM work. Interplanar spacings that were characteristic of only two zirconia structures, monoclinic and orthorhombic (cotunnite), were found. These interplanar spacings calculated from the HRTEM images were consistent with either the tetragonal (P-42m) or orthorhombic II (21 Gpa, Pnma) phases. There were, however, six values of interplanar spacings observed in the samples (Table 3) which are characteristic only of the orthorhombic and monoclinic structures. Since the single particle electron diffraction patterns (Fig. 3) had eliminated the monoclinic structure, this result again strongly suggested the presence of the high temperature and pressure orthorhombic structure for the synthesized zirconia. These interplanar spacings were found for all but one of the synthesized samples (1600-μL HNO_3).

Heat treatment of zirconium oxide

Several of the sol–gel-derived zirconia powder samples were heat treated to determine the thermal stability of the phases identified in the as-synthesized powders. Five separate samples of zirconium oxide powders, synthesized using 1200 μl of 0.94-M nitric acid, zirconium (IV)-*n*-butoxide and anhydrous 1-butanol, were heat treated at 473, 673, 873, 1073, and 1273 K in a furnace open to the atmosphere for a period of 1 h. XRD analysis of the sample heat treated at 473 K showed little change from the as-synthesized material shown in Fig. 2a. At 673 K (Fig. 4a), the initiation of a phase transition was suggested by the broadening of the peak centered at 2Θ of 30°. Particle sizes were still too small for the pattern to provide clear structural information. Following heat treatment at 873 K, however, the sample showed clear evidence of transformation to the tetragonal phase as shown in Fig. 4b. For the 1073 K sample (Fig. 4c), the tetragonal phase remained dominant, but the characteristic peaks for the monoclinic structure had begun to emerge. At 1273 K, the material had transformed completely to the monoclinic structure as shown in Fig. 4d.

Further characterization of the transformation of these samples with heat treatment was conducted using a concurrent TGA/DTA analysis (Fig. 5a) run in a closed, sealed chamber, maintaining the same argon atmosphere throughout the run. The samples were synthesized using 2000 μL of 0.94-M nitric acid. This limited the supply of oxygen and/or moisture to the as-synthesized sample to that initially present when the gas was introduced. Temperature increase was 10 K/min. The test was used to obtain data on simultaneous weight loss and phase transformations for the same sample. The analysis was conducted over the temperature range 278 to 1773 K. At approximately 373 K, an endothermic peak is found and approximately 10% of the materials weight was lost, suggesting a small loss of moisture and/or alcohol from the interstitial regions between the crystallites. Subsequent heating of the system lead to the loss of approximately another 60% of the material. This was most likely the loss of the remaining unreacted zirconium (IV)-*n*-butoxide. Beyond 463 K, sample weight decreased by only 2% for the remainder of the run. The remainder of the DTA curve displayed no other thermal events, indicating that no phase transitions had occurred in the material.

To determine the effect of different atmospheres for the same sample, under identical thermal conditions, powders synthesized at 2000 μL of 0.94-M nitric acid were sent to a commercial laboratory to be examined under both flowing argon and air. Each DTA returned the same results,

Table 3 The interplanar spacing of other than tetragonal zirconia determined from HRTEM micrographs

Nitric acid volume [HNO_3] (μL)	Sample interplanar spacing (Å)	Closest interplanar spacing for each structure (Å)	Structure for best interplanar spacing fit	Peak intensity (%)
2000	3.12-3.15	3.16	Monoclinic or orthorhombic (21 Gpa)	100
1600	Indeterminable	Indeterminable	Indeterminable	N/A
1200	3.26	3.24	Orthorhombic (21 Gpa)	20
800	3.23	3.24	Orthorhombic (21 Gpa)	20
400	3.23	3.24	Orthorhombic (21 Gpa)	20

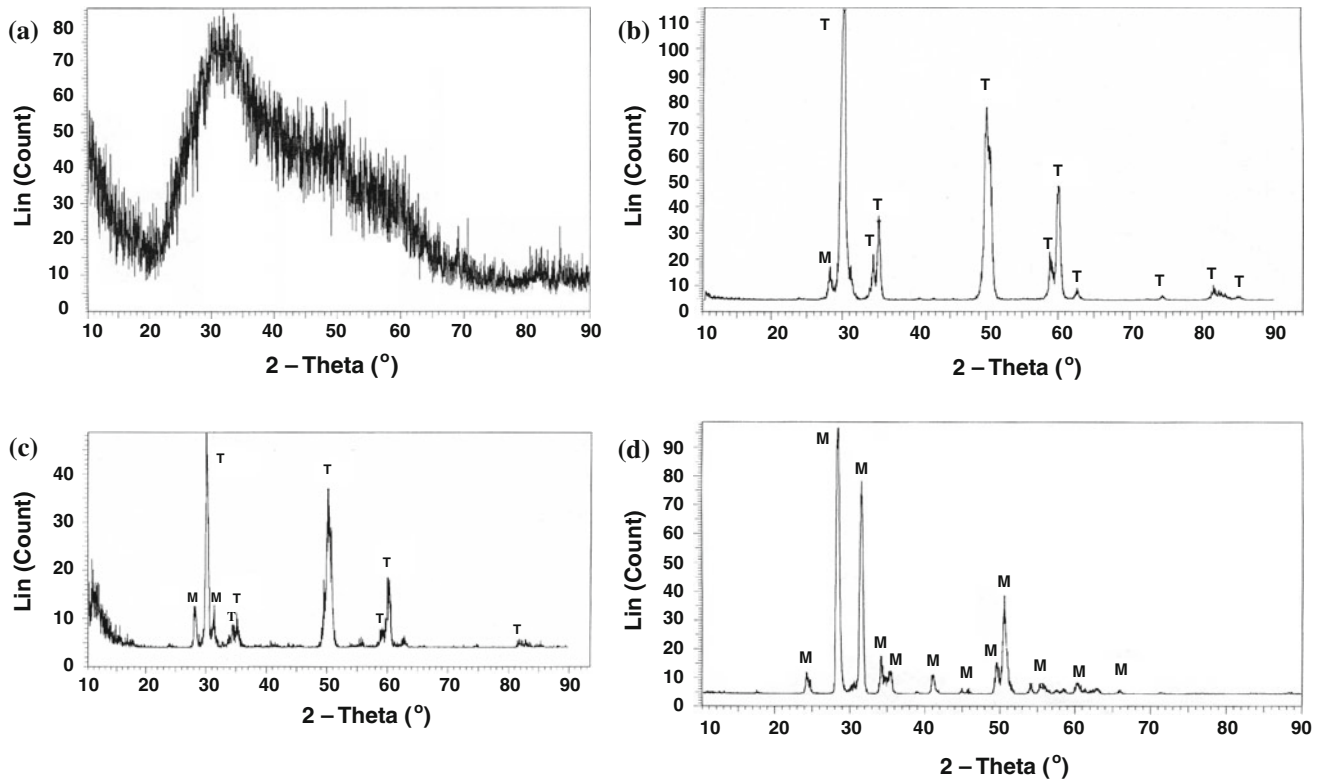

Fig. 4 **a** X-ray diffraction pattern for as-synthesized zirconia powder treated at **a** 673 K for 1 h open to atmosphere, **b** 873 K for 1 h open to atmosphere, with the monoclinic (*M*) and tetragonal (*T*) peaks indicated, **c** 1073 K for 1 h open to atmosphere, with the monoclinic (*M*) and tetragonal (*T*) peaks indicated, and **d** 1273 K for 1 h open to atmosphere, with the monoclinic (*M*) peaks indicated

indicating phase transformations had occurred, therefore only the sample examined under argon is shown in Fig. 5b. An endothermic peak was found at approximately 400 K, indicative of the loss of trapped water and/or alcohol within the interstitial pores. Starting at 454 K exothermic peaks were found. The only difference between Fig. 5a and b was the constant influx of air/argon during the tests which were not specifically treated to remove any small amounts of oxygen and/or moisture present. As the analytical grade of argon gas used at HTML at ORNL was found to posses $\sim$30 ppm of O_2, by volume, it is not unreasonable to suggest that the argon used at the commercial laboratory where the results in Fig. 5b were obtained was comparably contaminated.

To further investigate the effect of oxygen on the zirconia structure, samples from the same batch were studied under varying conditions using high-temperature XRD, these being (1) air, (2) ungettered argon ($\sim$30 ppm O_2), (3) gettered argon (0 ppm O_2), and (4) vacuum. The same sample was used for all four runs and was synthesized under conditions of 2000 μL of 0.94-M HNO_3 and dried at low temperature. The first run was done in air (20% O_2, 80% N_2) to obtain a reference XRD pattern (Fig. 6a). The dominant structure is tetragonal, but a careful examination of the data at $T = 1073$ K suggests a pair of convoluted peaks at $2\Theta = 33°$ only found in the Ortho I XRD pattern. That these peaks are indicative of the Ortho I structure is further supported by the fact that they are not present in the XRD pattern taken at $T = 1173$ K, suggesting that the sample has undergone a phase transition. In addition, the two strongest characteristic peaks for the monoclinic structure, found at $2\Theta = 27.84°$ and 31.18°, are clearly seen on either side of the strongest tetragonal peak at $2\Theta = 30°$. As the temperature increases, the peaks increase in intensity, becoming most pronounced at 1273 K. By 1373 K, these peaks have disappeared, indicating that the structure has completely reverted to the stable tetragonal structure typically found at that temperature and ambient pressure.

The next set of high-temperature XRD runs were under ungettered argon (Fig. 6b), possessing approximately 30 ppm O_2. Since the only two monoclinic peaks formed during the air run in air (Fig. 6a) were found between $2\Theta = 25°$ and 35°, only this portion of the patterns are shown. From Fig. 6b, it can be clearly seen that the characteristic monoclinic peaks found at $2\Theta = 27.84°$ and 31.18° are clearly present at $T = 1073$, 1173, and 1273 K, indicating the presence of the monoclinic phase. It was

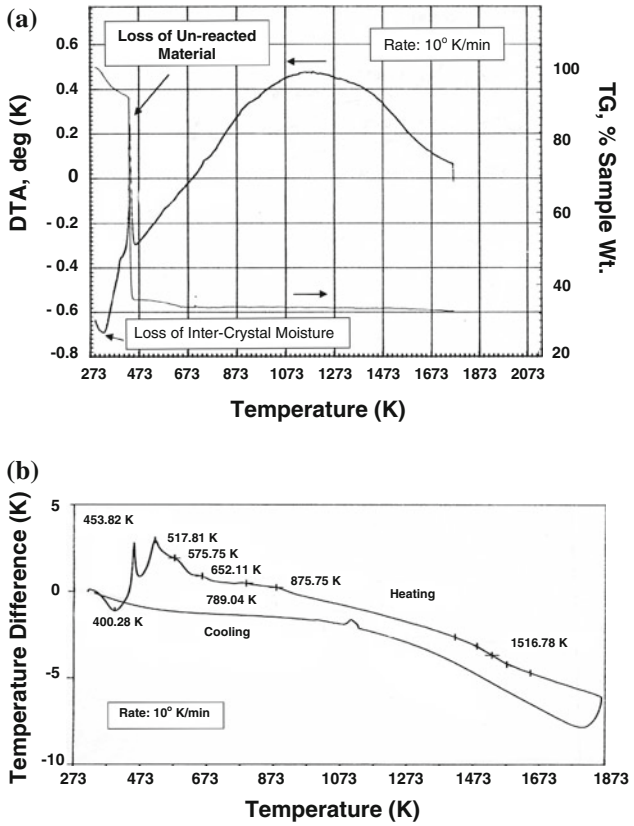

Fig. 5 **a** Concurrent DTA and TGA performed in a closed, sealed chamber under argon of as-synthesized zirconia at a concentration of 2000 μL 0.94-M nitric acid. **b** DTA performed under flowing argon of as-synthesized zirconia at a concentration of 2000 μL of 0.94-M nitric acid from M&P Labs

necessary to significantly enlarge Fig. 6b to clearly present the monoclinic peaks as they were significantly smaller than those found in Fig. 6a.

The next step was to remove as much of the O_2 present in the argon gas as possible by passing it through a getter to reproduce the conditions present in the DSC/TGA in Fig. 4a. XRD patterns were run at temperatures from 298 to 1673 K under gettered argon. The XRD patterns made at $T = 1073$, 1173, 1273, and 1373 K are presented in Fig. 6c. It can easily be observed that the characteristic $2\Theta = 27.74°$ and 31.18° indicative of the monoclinic phase are not present in any of the XRD patterns.

The next sample was run under vacuum (Fig. 6d). Peaks for the tetragonal structure were clearly defined at 663 K and the XRD pattern and did not change through 1273 K. Under ungettered argon and air (Fig. 6b), where oxygen and/or moisture was available to the sample, XRD peaks for the monoclinic phase were found to form at approximately 1073 K and became increasingly evident as the temperature increased. By 1273 K, the monoclinic peaks were most pronounced. By 1373 K, all evidence of the monoclinic structure has disappeared, leaving only the tetragonal structure. Therefore, when air and/or moisture were available, the monoclinic phase of zirconia was found to form, while under vacuum (Fig. 6d) and gettered argon (Fig. 6c), there was an insufficient amount of oxygen and/or moisture to allow the material to begin transforming to the monoclinic structure. The sample instead remained in the tetragonal phase throughout the entire temperature range.

BET nitrogen adsorption surface areas for these samples are reported in Table 2, and are consistent with an average primary particle size of approximately 5 nm. The increase in surface area with initial heat treatment is attributed to elimination of any residual alcohol, water and/or gel that may have blocked access to the particle surface. The temperature range from 273 to 473 K, where the greatest increase in surface area occurs is consistent with peaks and weight loss found in Fig. 5a, which is suggestive of the gel evaporating from around the crystallites. The decrease in surface area observed at the 873 and 1073 K temperatures is consistent with growth of the primary particles themselves. These results are reflected in the XRD patterns (Fig. 4b, c), which present clearly delineated peaks due to the growth of the primary particles.

Crystallites of identical diameters, including those synthesized in this study, have been produced for four of the polymorphs of ZrO_2 [16, 18, 32] without stabilizing agents. This suggests another factor than surface energy as the root cause of the metastable structures of zirconia. Work done in the 1970s by Hoskins and Martin on defect fluorite structures, including zirconia, suggest that the number and placement of oxygen vacancies [33–35] as the factor determining the structure of the material. This is also supported in the study by Lu et al. [36], who demonstrated the effect of differing population sizes of vacancies on the stability and transformation of the metastable tetragonal structure to the monoclinic structure at low temperatures. The results presented in this article also demonstrates that under identical conditions, where air and/or moisture is not present, the XRD spectra of tetragonal zirconia shows no formation of a monoclinic phase in the thermal region above 623 K. Where oxygen is present, even at ~30 ppm O_2, the monoclinic phase does begin to form above 623 K. Therefore, the structure of the synthesized zirconia appears to be linked to the oxygen vacancy population and placement within the material [33–35].

Summary and conclusions

Orthorhombic and tetragonal zirconias have been synthesized at ambient pressure and temperature using a dilute sol–gel method under high-acid low-moisture conditions. The size and resultant phase of the particles was found to

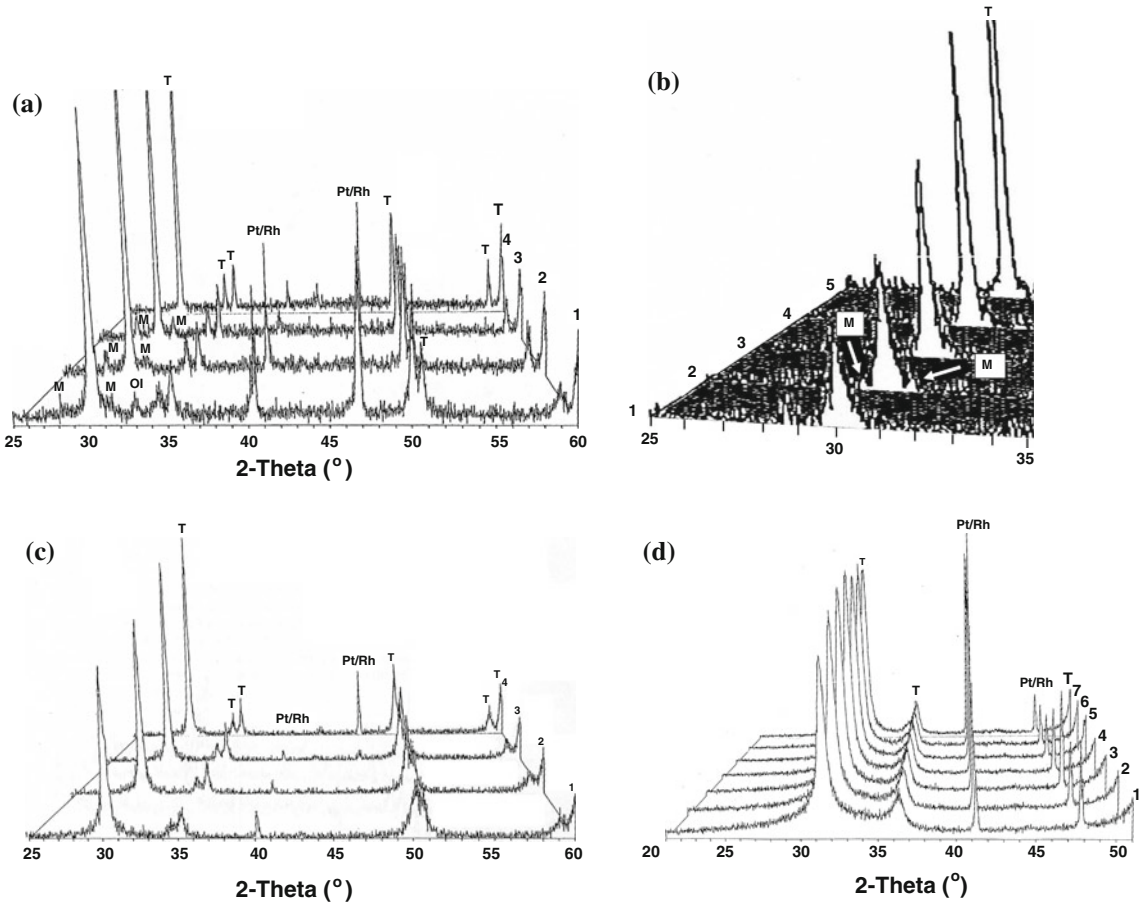

Fig. 6 **a** High-temperature XRD patterns in an environmental chamber for material treated under air at: (1) 1073 K, (2) 1173 K, (3) 1273 K, (4) 1373 K, with orthorhombic I (*OI*), monoclinic (*M*), tetragonal (*T*), and platinum/rhenium (*Pt*/*Rh*) peaks indicated. **b** High-temperature XRD patterns in an environmental chamber for material treated under argon at (1) 973 K, (2) 1073 K, (3) 1173 K, (4) 1273 K, (5) 1373 K, with monoclinic (*M*) and tetragonal (*T*) peaks indicated. **c** High-temperature XRD patterns in an environmental chamber for material treated under gettered argon at: (1) 1073 K, (2) 1173 K, (3) 1273 K, (4) 1373 K, with tetragonal (*T*) and platinum/rhenium (*Pt*/*Rh*) peaks indicated. **d** High-temperature XRD patterns in an environmental chamber for material treated under vacuum at: (1) 1073 K, (2) 1123 K, (3) 1173 K, (4) 1223 K, (5) 1273 K, (6) 1323 K, (7) 1373 K, with monoclinic (*M*), tetragonal (*T*) and platinum/rhenium (*Pt*/*Rh*) thermocouple peaks are indicated

be sensitive to system acid concentration and moisture content, with the most acidic conditions/lowest moisture producing the smallest particles and the orthorhombic phase as determined by electron diffraction analysis of single particles.

At lower acid concentrations and higher moisture content, the tetragonal phase was produced at ambient conditions, as determined by XRD analysis. Heat treatment of the samples resulted in complete transformation of the powder to the tetragonal phase, with treatment at the highest temperature of 1273 K resulting in transformation to the monoclinic phase. Particle size, however, varied only slightly with heat treatment; with the largest primary particle diameters reported being approximately 7.5 nm in samples heat treated at 1073 and 1273 K. At this size these crystallites should possess the metal-stable tetragonal structure, not monoclinic, according to Garvie [17, 18]. Zirconia heated under conditions where it was denied sufficient oxygen and/or moisture remained in the tetragonal structure between 873 and 1373 K, where it would normally transform to the monoclinic structure if unstabilized.

Acknowledgements Supported by the U.S. Department of Energy under UCR grant DE-FG26-97FT97260. Supported by work at the High Temperature Materials Laboratory at Oak Ridge National Laboratory with assistance from Karren L. More and Claudia J. Rawn.

References

1. Abriata JP, Garces J, Versaci R (1986) Bull Alloy Phase Diagr 7(2):116
2. Levin EM, McMurdie HF (1975) Phase diagrams for ceramists, supplement. The American Ceramic Society, Inc., Columbus #4259

3. Arashi H, Ishigame M (1982) Phys Stat Sol (a) 71:3130
4. Lityagina LM, Kabalkina SS, Pashinka TA, Khozyainov AI (1978) Sov Phys Solid State 20(11):2009
5. Ohtaka O, Yamanaka T, Kume S (1991) J Am Ceram Soc 74(3):505
6. Dewhurst JK, Lowther JE (1998) Phys Rev B 57(2):741
7. Ohtaka O, Kume S, Awami T, Urabe K (1988) J Am Ceram Soc 71(3):C164
8. Bloch S, Da Jornada JAH, Piermarini GJ (1985) J Am Ceram Soc 68:497
9. Kisi EH, Howard CJ (1989) J Am Ceram Soc 72(9):1757
10. Suyama R, Ashida TT, Kume S (1985) J Am Ceram Soc 68(12):C314
11. Devi SRU, Ming LC, Manghnani MH (1987) J Am Ceram Soc 70(9):C218
12. Leger JM, Tomaszewski PE, Atouf A, Pereira AS (1993) Phys Rev B 47:14075
13. Inter. Cent. Diff. Data, Powd. Diff. File #37-1413
14. Inter. Cent. Diff. Data, Powd. Diff. File #83-0810
15. Ruff O, Ebert FZ (1929) Anorg Allgem Chem 180:19
16. Clearfield A (1964) Inorg Chem 3(1):146
17. Garvie RC (1965) J Phys Chem 69(4):1238
18. Garvie RC (1978) J Phys Chem 82(2):218
19. Schultz M, Grimm S, Burckhardt W (1993) Solid State Ionics 63–65:18
20. Ramamurthi SD, Xu Z, Payne DA (1990) J Am Ceram Soc 73(9):2760
21. Okubo T, Nagamoto H (1995) J Mater Sci 30(3):749. doi: 10.1007/BF00356338
22. Suyama R, Takubo H, Kume S (1985) J Am Ceram Soc 68(9):C237
23. Pissenberger A, Gritzner G (1995) J Mater Sci Lett 14:1580
24. Guinebretiere R, Oudjedi Z, Dauger A (1996) Scripta Mater 34(7):1039
25. Rossignol S, Madier Y, Duprez D (1999) Catal Today 50:261
26. Trolliard G, Benmechta R, Mercurio D (2007) Acta Mater 55:6011
27. Ogihara T, Mizutani N, Kato M (1989) J Am Ceram Soc 72(3):421
28. Cullity BD (1978) Elements of X-ray diffraction, 2nd edn. Addison-Wesley Publishing Company Inc., Reading
29. Inter. Cent. Diff. Data, Powd. Diff. File #41-0017
30. Inter. Cent. Diff. Data, Powd. Diff. File #42-1164
31. Steele JK, Biederman RR (1991) Mater Charact 27:213
32. Hu MZC, Harris MT, Byers Ch H (1998) J Coll Interface Sci 198:87
33. Martin RL (1974) J Chem Soc Dalton 1335
34. Hoskins BF, Martin RL (1975) J Chem Soc Dalton 576
35. Hoskins BF, Martin RL (1976) J Chem Soc Dalton (1976) 676
36. Lu X, Lian K, Gu S, Zhen Y, Fang H (1997) J Mater Sci 32:6653. doi:10.1023/A:1018604504171